

## Einstein-Podolsky-Rosen Paradox in Twin Images

Paul-Antoine Moreau, Fabrice Devaux, and Eric Lantz

*Département d'Optique, Institut FEMTO-ST, Université de Franche-Comté, CNRS, 25000 Besançon, France*

(Received 9 May 2014; published 14 October 2014)

Spatially entangled twin photons provide both promising resources for modern quantum information protocols, because of the high dimensionality of transverse entanglement, and a test of the Einstein-Podolsky-Rosen paradox in its original form of position versus impulsion. Usually, photons in temporal coincidence are selected and their positions recorded, resulting in *a priori* assumptions on their spatiotemporal behavior. In this Letter, we record, on two separate electron-multiplying charge coupled devices cameras, twin images of the entire flux of spontaneous down-conversion. This ensures a strict equivalence between the subsystems corresponding to the detection of either position (image or near-field plane) or momentum (Fourier or far-field plane). We report the highest degree of paradox ever reported and show that this degree corresponds to the number of independent degrees of freedom, or resolution cells, of the images.

DOI: 10.1103/PhysRevLett.113.160401

PACS numbers: 03.65.Ud, 42.50.Ar, 42.50.Dv, 42.50.Xa

In 1935, Einstein, Podolsky and Rosen (EPR) showed [1] that quantum mechanics predicts that entangled particles could have both perfectly correlated positions and momenta, in contradiction with the so-called local realism where two distant particles should be treated as two different systems. Though the original intention of EPR was to show that quantum mechanics is not complete, the standard present view is that entangled particles do experience nonlocal correlations [2–4]. It can be shown that the spatial extent of these correlations corresponds to the size of a spatial unit of information, or mode, offering the possibility of detecting high dimensional entanglement in an image with a sufficient number of resolution cells [5,6]. However, in most experiments the use of single photon detectors and coincidence counting leads to the detection of a very few parts of the selected photons, generating a sampling loophole. High sensitivity array detectors have been used outside the single photon-counting regime in order to witness quantum features of light [7,8]. However, the EPR paradox is intimately connected to the particle character of light and its detection should involve single photon imaging, possible either with intensified charge coupled devices able to isolate pairs of entangled photons [9,10] or, more recently, electron-multiplying charge coupled devices (EMCCDs) [11].

Because of their high quantum efficiency EMCCDs allowed the demonstration of sub-shot-noise correlations in far-field images of spontaneous parametric down-conversion (SPDC) [12,13]. More recently, two experiments intended to achieve the demonstration of an EPR paradox or EPR correlations in couples of near-field and far-field images recorded with in an EMCCD. The first experiment in our group involved the detection of twin images on a single camera, by separating in the near field the cross-polarized photons with a polarizing beam splitter, inducing some overlap of the near-field images and a rather small

resolution in the far field because of walk-off. The results exhibited a low degree of paradox, far from the theoretical values, though highly significant and in accordance with the full-field requirements [14]. The second experiment [15] exhibited also both near-field and far-field correlations, with a much lower product of the spatial extents. However, because of type-I phase matching, photons of a pair were detected on the same coherence area in the near field. As a consequence, pairs that were incident on the same pixel did not participate to the experimental correlation, because of the on-off character of the detection, and results were obtained for only one dimension because of the smearing effects between adjacent pixels. More fundamentally, the absence of spatial separation makes that the two parts of the wave function corresponding to the two photons are spatially superposed in the near field, while a demonstration of an EPR paradox implies detection of remote correlations. Hence, the authors claimed observation of EPR-type correlations rather than an EPR paradox.

In the present experiment, the use of two cameras allows a separation of the twin images without any further optical component, thanks to walk-off, and a perfect identity of the subsystems corresponding to far-field and near-field detection, except the position of the imaging systems composed on each arm of a lens and a camera. Before describing our experimental results, let us recall that an EPR paradox arises when correlations violate an inequality corresponding to the Heisenberg uncertainty principle if applied to a single particle 1 or 2, but expressed in terms of conditional variances [16,17]:

$$\langle \Delta^2(\rho_1 - \rho_2) \rangle \langle \Delta^2(p_1 + p_2) \rangle \geq \frac{\hbar^2}{4}, \quad (1)$$

where  $\rho_i$  is the transverse position of photon  $i$  ( $i = 1, 2$ ) in the middle plane of the crystal and  $p_i$  its transverse

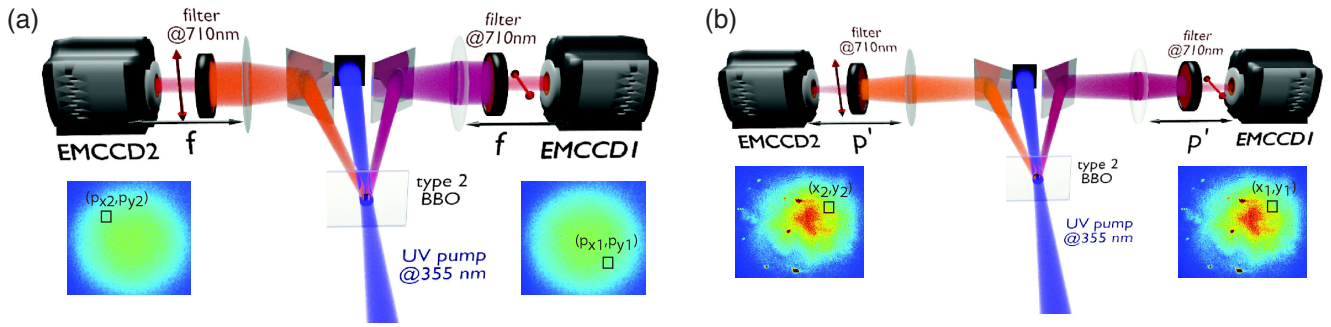


FIG. 1 (color online). Experimental setups used to image correlations. (a) Measurement of momentum correlations with the cameras in the focal plane. Inserts: sums of 700 far-field images;  $px_1 = -px_2$ ,  $py_1 = -py_2$  are the coordinates of twin pixels. (b) Cameras in the crystal image plane and sums of 700 near-field images with twin pixels in  $x_1 = x_2$ ,  $y_1 = y_2$ .

momentum. In order to make the demonstration consistent, the statistical evaluation of the variances should be made on the same system in the near and the far field. By using two EMCCD cameras that detect photons in the whole SPDC field, we ensured this consistency. By approximating the phase matching function of SPDC to a Gaussian, the wave function of the biphoton can be written [18]

$$\Psi(\boldsymbol{\rho}_1, \boldsymbol{\rho}_2) = N \exp\left(-\frac{|\boldsymbol{\rho}_1 + \boldsymbol{\rho}_2|^2}{4\sigma_p^2}\right) \exp\left(-\frac{|\boldsymbol{\rho}_1 - \boldsymbol{\rho}_2|^2}{4\sigma_\phi^2}\right), \quad (2)$$

$$\Psi(\boldsymbol{p}_1, \boldsymbol{p}_2) = \frac{1}{N\pi^2} \exp\left(-\sigma_p^2 \frac{|\boldsymbol{p}_1 + \boldsymbol{p}_2|^2}{4\hbar^2}\right) \exp\left(-\sigma_\phi^2 \frac{|\boldsymbol{p}_1 - \boldsymbol{p}_2|^2}{4\hbar^2}\right), \quad (3)$$

where  $N$  is a normalization constant,  $\boldsymbol{\rho}_i = (x_i, y_i)$ ,  $\boldsymbol{p}_i = (p_{xi}, p_{yi})$ ,  $\sigma_p$  the standard deviation of the Gaussian pump beam, and  $\sigma_\phi$  the standard deviation, defined in the near field, of the Fourier transform of the phase matching function defined in the far field. In our experimental conditions where  $\sigma_p \gg \sigma_\phi$ , these equations show that the product of conditional variances is equal to

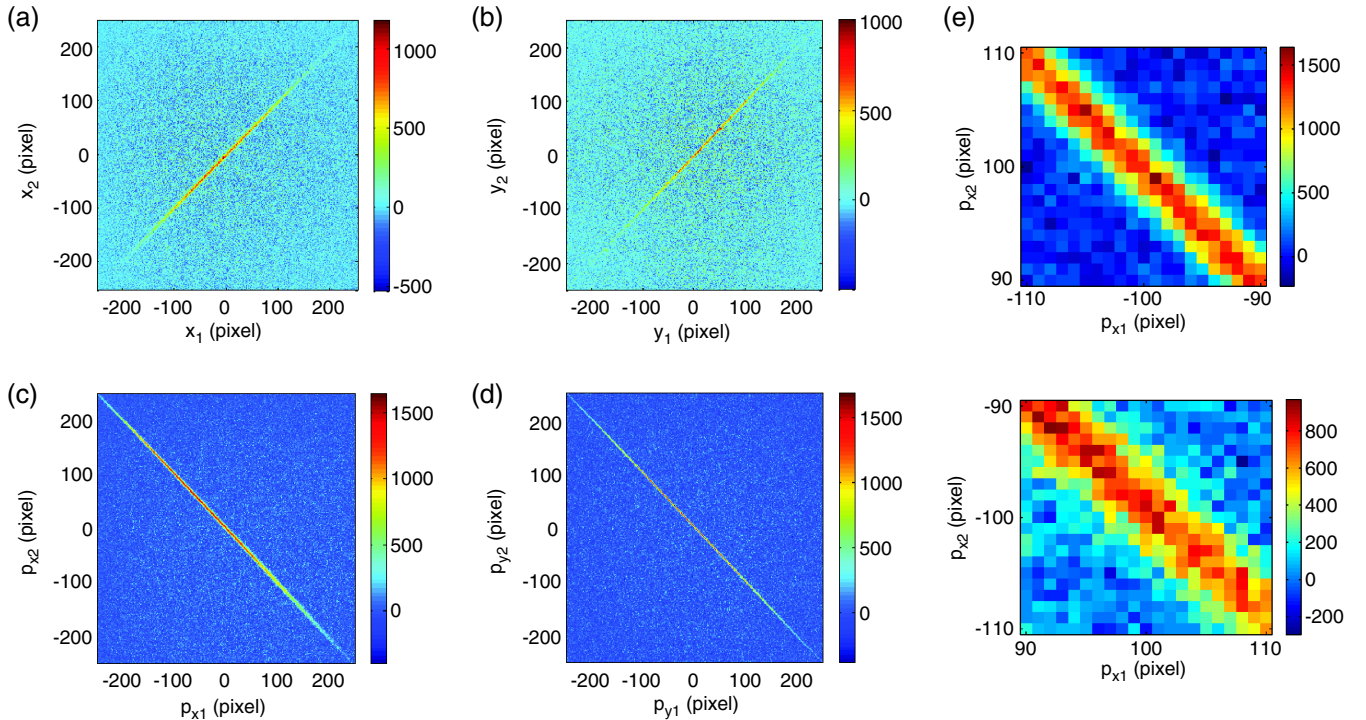


FIG. 2 (color online). Joint probabilities versus the transverse spatial coordinates. Color scales are expressed in coincidence counts over 35 000 pairs of images, corrected from the mean corresponding to accidental coincidences: (a),(b) near field; (c),(d) far field. (e) In the far field, the correlations arise in a coherence area that is larger for momenta the most distant from the pump direction, in the direction  $x$  along which the two fluorescence beams are separated from the walk-off.

$$\langle \Delta^2(\rho_1 - \rho_2) \rangle \langle \Delta^2(p_1 + p_2) \rangle = \hbar^2 \frac{\sigma_\phi^2}{\sigma_p^2} = \frac{\hbar^2}{4V}, \quad (4)$$

where  $V$  is defined by this equation as the degree of paradox. Using the results of Law and Eberly [19], it can be shown that  $V$  is also the Schmidt number of the entanglement [20], i.e., the whole dimensionality of the biphoton in the two-dimensional transverse space. For a one-dimensional system of length corresponding to the lateral size of the bidimensional one, the Schmidt number becomes equal to the square root of that of the bidimensional system. Hence,  $V$  becomes the square of this Schmidt number [21].

The experimental setup is shown in Fig. 1. Pump pulses at 355 nm provided by a 27 mW laser illuminated a 0.6-mm long  $\beta$  barium borate (BBO) nonlinear crystal cut for type-II phase matching. The signal and idler photons were separated by means of two mirrors and sent to two independent imaging systems. The far-field image of the SPDC was formed on the EMCCDs placed in the focal plane of two 120-mm lenses, Fig. 1(a). In the near-field configuration, Fig. 1(b), the plane of the BBO crystal was imaged on the EMCCDs with a transversal magnification  $M = 2.47 \pm 0.01$ . Note that only the positions of the lenses and cameras are different in the two configurations. The

back-illuminated EMCCD cameras (Andor iXon3) have a quantum efficiency greater than 90% in the visible range. The detector area is formed by  $512 \times 512$  pixels, with a pixel size of  $s_{\text{pix}} = 16 \times 16 \mu\text{m}^2$ . We used a readout rate of 10 MHz at 14 bits, and the cameras were cooled to  $-100^\circ\text{C}$ . An image corresponds to the summation of 100 laser shots, i.e., an exposure time of 0.1 s and a dead time between two successive images of about the same value, in order to allow a perfect synchronization between both cameras. Measurements were performed for a crystal orientation corresponding to noncritical phase matching at degeneracy, i.e., collinear orientation of the signal and idler Poynting vectors in the crystal [22]. Photon pairs emitted around the degeneracy were selected by narrow-band interference filters centered at 710 nm ( $\Delta\lambda = 4$  nm). The photon-counting regime was ensured by adjusting the exposure time in such a way that the mean fluency of SPDC was between 0.1 and 0.2 photon per pixel in order to minimize the whole number of false detections [11]. The mean number of photons per spatiotemporal mode was less than  $10^{-3}$ , in good agreement with the hypothesis of pure spontaneous parametric down-conversion, without any stimulated amplification. We applied a thresholding procedure [11] to convert the gray scales into binary values that

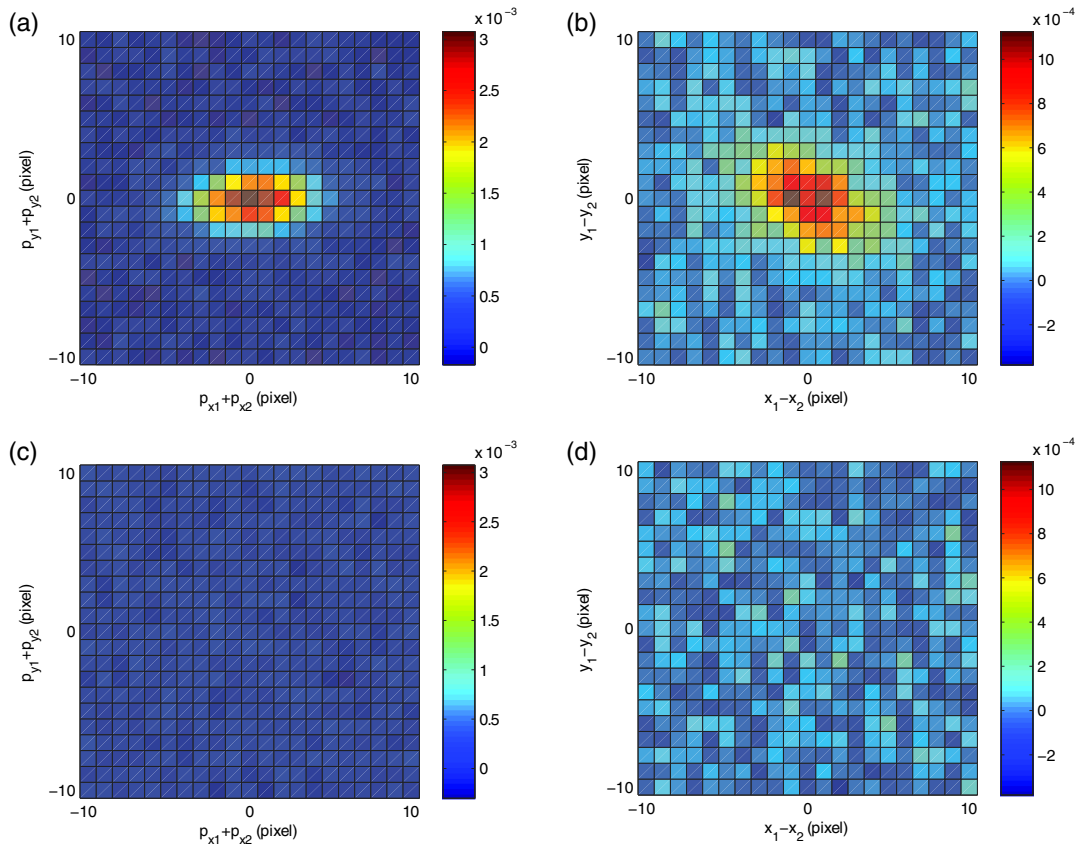


FIG. 3 (color online). Normalized cross-correlation functions in position and momentum: The cross-correlation is calculated over 700 images in the far field (a),(c) and image plane (b),(d). In (c) and (d) are presented cross-correlation of images that do not share any pump pulses.

TABLE I. Inferred variances.

Variances	Measured values
$\Delta^2(x_1 - x_2)$	$299 \pm 14 \mu\text{m}^2$
$\Delta^2(y_1 - y_2)$	$168 \pm 7 \mu\text{m}^2$
$\Delta^2(p_{x1} - p_{x2})$	$(9.70 \pm 0.1) \times 10^{-6} \hbar^2 \mu\text{m}^{-2}$
$\Delta^2(p_{y1} - p_{y2})$	$(2.53 \pm 0.04) \times 10^{-6} \hbar^2 \mu\text{m}^{-2}$

correspond to 0 or 1 photon. The conditional probability distributions calculated using 35 000 images are shown in Fig. 2. The correlation profiles agree with the theoretical expectations (2) and (3) with  $\sigma_p \gg \sigma_\phi$ .

We have shown [23] that the conditional variances  $\langle \Delta^2(\rho_1 - \rho_2) \rangle$  and  $\langle \Delta^2(p_1 + p_2) \rangle$  correspond to the widths of the normalized cross-correlation of photodetection images, after subtraction from these images of their deterministic part, i.e., the mean of the images shown in the insets of Fig. 1. Because of this subtraction, the spots observed in the near-field insets, due to tiny defaults on the BBO crystal, do not lead to deterministic correlations; see Fig. 3(d). The experimental values obtained by fitting the normalized cross-correlations presented in Fig. 3 are reported in Table I, for the two orthogonal directions of the transverse plane  $x$  and  $y$ .

Using the measured values given in Table I, we find the following product of conditional variances:

$$\Delta^2(x_1 - x_2)\Delta^2(p_{x1} + p_{x2}) = (2.9 \pm 0.2) \times 10^{-3} \hbar^2, \quad (5)$$

$$\Delta^2(y_1 - y_2)\Delta^2(p_{y1} + p_{y2}) = (4.2 \pm 0.2) \times 10^{-4} \hbar^2. \quad (6)$$

These results clearly violate inequality (1), thus exhibiting an EPR paradox in the two transverse dimensions. Moreover, the results are in rather good agreement with the theoretical expectations  $8.6 \times 10^{-4} \hbar^2$  on  $x$  and  $2.6 \times 10^{-4} \hbar^2$  on  $y$  obtained by a numerical computation that takes into account the effect of the width of the interference filter. This effect explains the anisotropy shown in Fig. 2(e), i.e., an enlargement in the  $x$  direction for the large values of  $x_1$ : for non perfect frequency-degenerate photons, the shift from perfect symmetry is proportional to the walk-off, as detailed in [23]. This effect should not be confounded with the anisotropy described in [24], that is due to an extraordinary strongly focused pump in a long uniaxial crystal. Note also that our numerical computation uses the exact sinc-like phase matching function and not its Gaussian approximation. By using Eq. (4), we find along  $x$  a degree of paradox of  $86 \pm 5$  and along  $y$  of  $595 \pm 40$ . To the best of our knowledge, this degree of 595 is the highest ever reported for an EPR paradox, whatever the considered domain. The former best values were 25 for quadrature experiments [25], 380 for the EPR correlations of Ref. [15], 128 in Ref. [5], and 100 by encoding with a spatial light modulator [26].

We show in Fig. 4 that the minimum number of images that allows a safe assessment of the correlation peaks in both spaces is of the order of 20. Indeed a quantum correlation peak is evidenced if it cannot be confounded,

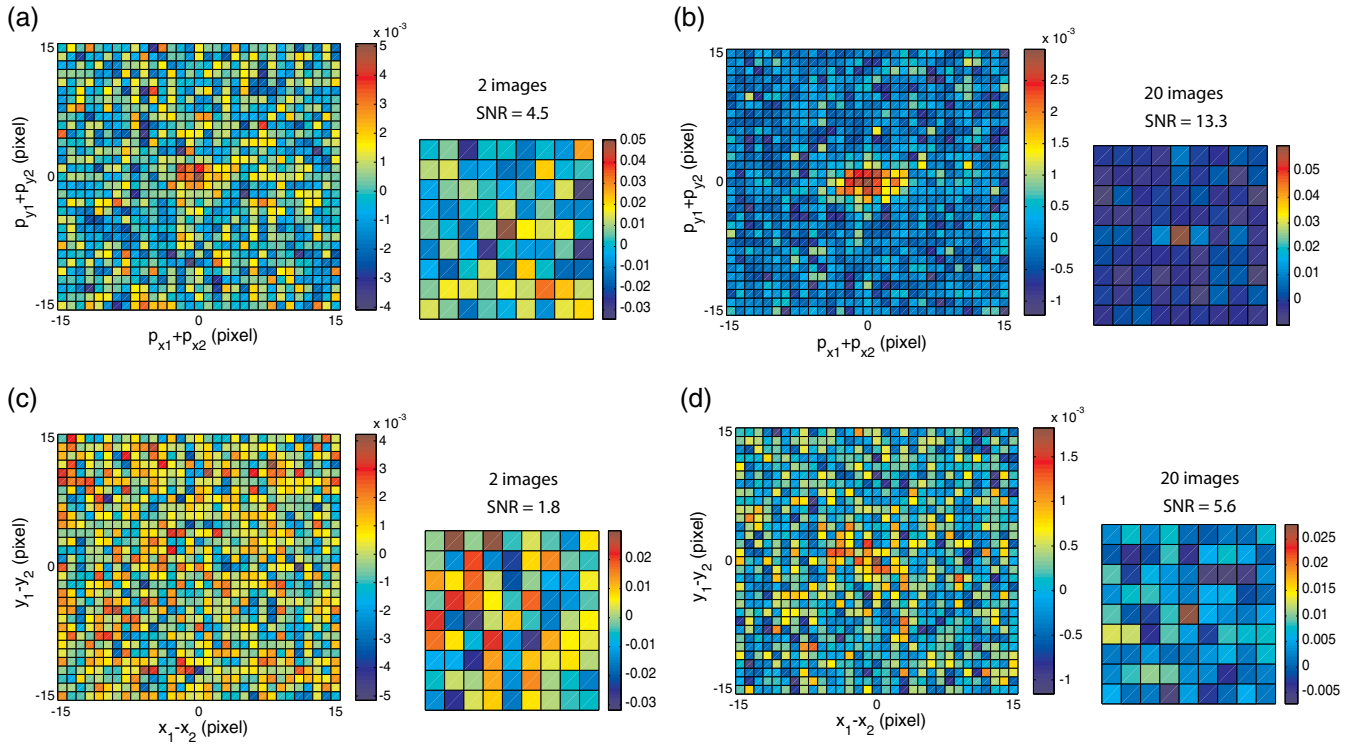


FIG. 4 (color online). Normalized cross-correlation function versus the number of images: left images show correlation computed on the physical pixels (only the central part is presented). Smaller right images show correlation computed after grouping  $8 \times 8$  pixels: (a),(b) far field; (c),(d) near field.

with high probability, with random fluctuations of the background noise. Without any *a priori* assumption on the position of the peak, this is ensured with a confidence of 99% if the magnitude of the true peak is greater than 4.5 standard deviations, for an image of  $64 \times 64$  pixels obtained by summing the correlations on groups of  $8 \times 8$  pixels. This grouping is performed in order to adapt the size of the effective pixel to the size of the correlation peak. In Fig. 4, we have defined the signal-to-noise-ratio (SNR) as the magnitude of the correlation peak divided by the standard deviation, after grouping, of the correlation image outside the peak area. The minimum number of images necessary to demonstrate entanglement is only two in the far field, where deterministic distortions appear to be smaller than in the image plane.

Finally, we have verified that the images exhibit a sub-shot-noise statistics in both the near field and the far field:  $r_n = 0.9975 \pm 0.0004$  and  $r_f = 0.9959 \pm 0.0003$ , where  $r$  is defined by

$$r = \frac{\langle \Delta^2(N_1 - N_2) \rangle}{\langle N_1 + N_2 \rangle}, \quad (7)$$

that is, the variance of the photon number difference  $N_1(\boldsymbol{\rho}) - N_2(\boldsymbol{\rho})$  [and  $N_1(\boldsymbol{\rho}) - N_2(-\boldsymbol{\rho})$  in far field] normalized to be expressed in shot noise units. These experimental results are under the classical limit 1, respectively, by more than 5 and 10 standard deviations, witnessing the quantum, i.e., particlelike, character of the correlations [12]. Note that smaller values of  $r$  can be obtained by grouping the pixels [23].

To conclude, we have demonstrated a two dimensional EPR paradox in the closest form of its original proposal by recording the behavior of light in couples of twin images. The quantum character of these images has been doubly demonstrated first by full-field measurement of a high degree of EPR paradox for both transverse directions, and second by demonstrating subshot noise character in both the near field and the far field. Reliable results can be obtained with 20 images, i.e., an acquisition time of 4 s and a computation time that scales also in seconds since cross-correlations are computed using FFT algorithms. This should be compared to days for raster scanning, or hours for compressive sensing [27]. Because of the experimental anisotropy, the dimensionality of entanglement, or Schmidt number  $K$ , can be assessed as the square root of the product of the paradox degrees in each direction:  $K = \sqrt{594 \times 85} = 225$ . Such high-dimensionality spatial entanglement has applications in numerous fields of quantum optics, like quantum cryptography [28] or quantum computation [29].

This work was partly supported by the Labex ACTION program (ANR-11-LABX-0001-01).

[1] A. Einstein, B. Podolsky, and N. Rosen, *Phys. Rev.* **47**, 777 (1935).

- [2] J. S. Bell, *Physics* **1**, 195 (1964).  
 [3] A. Aspect, P. Grangier, and G. Roger, *Phys. Rev. Lett.* **47**, 460 (1981).  
 [4] K. Banaszek and K. Wodkiewicz, *Phys. Rev. A* **58**, 4345 (1998).  
 [5] P. B. Dixon, G. A. Howland, J. Schneeloch, and J. C. Howell, *Phys. Rev. Lett.* **108**, 143603 (2012).  
 [6] J. C. Howell, R. S. Bennink, S. J. Bentley, and R. W. Boyd, *Phys. Rev. Lett.* **92**, 210403 (2004).  
 [7] G. Brida, M. Genovese, and I. R. Berchera, *Nat. Photonics* **4**, 227 (2010).  
 [8] O. Jedrkiewicz, Y.-K. Jiang, E. Brambilla, A. Gatti, M. Bache, L. A. Lugiato, and P. Di Trapani, *Phys. Rev. Lett.* **93**, 243601 (2004).  
 [9] S. S. R. Oemrawsingh, W. J. van Drunen, E. R. Eliel, and J. P. Woerdman, *J. Opt. Soc. Am. B* **19**, 2391 (2002).  
 [10] R. Fickler, M. Krenn, R. Lapkiewicz, S. Ramelow, and A. Zeilinger, *Sci. Rep.* **3**, 1914 (2013).  
 [11] E. Lantz, J.-L. Blanchet, L. Furfaro, and F. Devaux, *Mon. Not. R. Astron. Soc.* **386**, 2262 (2008).  
 [12] J.-L. Blanchet, F. Devaux, L. Furfaro, and E. Lantz, *Phys. Rev. Lett.* **101**, 233604 (2008).  
 [13] J.-L. Blanchet, F. Devaux, L. Furfaro, and E. Lantz, *Phys. Rev. A* **81**, 043825 (2010).  
 [14] P.-A. Moreau, J. Mougín-Sisini, F. Devaux, and E. Lantz, *Phys. Rev. A* **86**, 010101 (2012).  
 [15] M. Edgar, D. Tasca, F. Izdebski, R. Warburton, J. Leach, M. Agnew, G. Buller, R. Boyd, and M. Padgett, *Nat. Commun.* **3**, 984 (2012).  
 [16] M. D. Reid, *Phys. Rev. A* **40**, 913 (1989).  
 [17] M. D. Reid, P. D. Drummond, W. P. Bowen, E. G. Cavalcanti, P. K. Lam, H. A. Bachor, U. L. Andersen, and G. Leuchs, *Rev. Mod. Phys.* **81**, 1272 (2009).  
 [18] D. S. Tasca, S. P. Walborn, P. H. Souto Ribeiro, F. Toscano, and P. Pellat-Finet, *Phys. Rev. A* **79**, 033801 (2009).  
 [19] C. K. Law and J. H. Eberly, *Phys. Rev. Lett.* **92**, 127903 (2004).  
 [20] M. P. van Exter, A. Aiello, S. S. R. Oemrawsingh, G. Nienhuis, and J. P. Woerdman, *Phys. Rev. A* **74**, 012309 (2006).  
 [21] M. Fedorov, Y. M. Mikhailova, and P. A. Volkov, *J. Phys. B* **42**, 175503 (2009).  
 [22] E. Lantz and F. Devaux, *J. Opt. A* **2**, 362 (2000).  
 [23] F. Devaux, J. Mougín-Sisini, P.-A. Moreau, and E. Lantz, *Eur. Phys. J. D* **66**, 192 (2012).  
 [24] M. V. Fedorov, M. A. Efremov, P. A. Volkov, E. V. Moreva, S. S. Straupe, and S. P. Kulik, *Phys. Rev. Lett.* **99**, 063901 (2007).  
 [25] S. Steinlechner, J. Bauchrowitz, T. Eberle, and R. Schnabel, *Phys. Rev. A* **87**, 022104 (2013).  
 [26] M. Krenn, M. Huber, R. Fickler, S. Lapkiewicz, S. Ramelow, and A. Zeilinger, *Proc. Natl. Acad. Sci. U.S.A.* **111**, 6243 (2014).  
 [27] G. A. Howland and J. C. Howell, *Phys. Rev. X* **3**, 011013 (2013).  
 [28] C. Branciard, E. G. Cavalcanti, S. P. Walborn, V. Scarani, and H. M. Wiseman, *Phys. Rev. A* **85**, 010301 (2012).  
 [29] D. S. Tasca, R. M. Gomes, F. Toscano, P. H. Souto Ribeiro, and S. P. Walborn, *Phys. Rev. A* **83**, 052325 (2011).